Optica Applicata, Vol. LII, No. 4, 2022
DOI: 10.37190/oa220406

Tunable terahertz all-dielectric linear-to-circular polarization conversion metasurface

XIACAO JU[1,2], WEIGUANG WANG[1,2], BINGCHAO LIU[4], YANZHAO HOU[1,3], HUASHUN WEN[5,6], DAQUAN YANG[1,2,*]

[1]School of Information and Communication Engineering,
Beijing University of Posts and Telecommunications, Beijing 100876, China

[2]State Key Laboratory of Information Photonics and Optical Communications,
Beijing University of Posts and Telecommunications, Beijing 100876, China

[3]National Engineering Laboratory for Mobile Network Technologies,
Beijing University of Posts and Telecommunications, Beijing 100876, China

[4]Lenovo Research, Beijing 100094, China

[5]State Key Laboratory on Integrated Optoelectronics, Institute of Semiconductors,
Chinese Academy of Sciences, Beijing 100083, China

[6]School of Electronic, Electrical and Communication Engineering,
University of Chinese Academy of Sciences, Beijing 100049, China

[*]Corresponding author: ydq@bupt.edu.cn

Terahertz (THz) linear-to-circular (LTC) polarization conversion plays a crucial role in imaging and 6G wireless communication. This paper will give an account of a thermally tunable THz LTC polarization converter by using the active all-dielectric metasurface. It consists of zirconium oxide (ZrO_2) microsphere resonators, active strontium titanate (STO) cladding, and flexible polyimide substrate. Through numerical simulation, the amplitude of the ellipticity of the proposed polarization converter at 0.265 THz is –1, indicating that perfect right-hand circular polarization (RHCP) wave is achieved. Meanwhile, the amplitude of the ellipticity is less than –0.8 between 0.247 and 0.278 THz (relative bandwidth is 12%). In addition, with the temperature changes of 180 K (from 200 to 380 K), the operating frequency of the converter can be tuned from 0.220 to 0.291 THz, a sensitivity about 39 GHz/100 K is achieved. Besides, the modulation depth of the ellipticity amplitude can achieve 92% at 0.220 THz, which demonstrates that the converter can output terahertz wave with different polarization states, and the device can be fabricated on a large scale. These perfect conversion performances show that the converter has potential applications in high-speed communication and imaging.

Keywords: terahertz waves, dynamically tunable, strontium titanate, polarization conversion, all-dielectric metasurface.

1. Introduction

Terahertz (THz) wave (0.1 to 10 THz) has attracted more attention in imaging, spectroscopy, environmental surveillance, remote sensing, high-resolution radars, and high-speed communication [1–5]. In particular the rapid development of high-speed communication and imaging has attracted wide attention from scholars [6–13]. To improve the performance of these THz devices, the circular polarization wave with robustness [14] and chirality [15] is essential and necessary. However, the THz waves are mostly linearly polarized [16, 17]. More importantly, the polarization control is one of the most basic functions of optical components such as polarizers, polarization beam splitters, and polarization converters [18]. Therefore, the THz linear-to-circular (LTC) polarization converters are of significance in the expansion of THz devices. Generally, the THz polarization converter is based on birefringent waveplates [19]. However, the major problems of bulky size, high losses, and narrow bandwidth of waveplate have limited their applications in integrated THz devices [20]. Conversely, as the periodic sub-wavelength planar array with unique electromagnetic properties [21–27], metasurface has provided greater freedom and better performance in THz polarization conversion devices.

Nowadays, researchers have proposed a variety of THz polarization converters based on metasurfaces. GRADY *et al*. first reported the reflective and transmissive polarization converter based on metasurface [27]. CHIANG and YEN proposed a transmission broadband polarization converter, including s-type metal split ring resonators [28]. Compared with the metal metasurface, the all-dielectric metasurface has the characteristics of low loss [29]. However, the disadvantage of narrow relatively bandwidth limits their applications. For example, the all-dielectric THz LTC polarization converter proposed by ZHU *et al*. achieved a relative bandwidth of about 5% [30]. Therefore, realizing a higher relative bandwidth is one of the goals of the all-dielectric polarization converter. In addition, designing general-purpose equipment with tunable functions is the top priority to promote the development of THz technology [31]. In particular the dynamic control of THz wave that realizes LTC polarization conversion plays an important role in wireless communication switches and modulators [32]. More importantly, the device with tunable functions can effectively expand the working bandwidth and modulate the polarization state of incident wave [33]. For instance, a metal-isolator-metal metasurface for THz polarization converter is proposed by VASIĆ *et al*., which achieved fast modulation in a switching time of about 10 ms [33]. However, due to the metal parts of metallic metasurfaces with the limits of easy breakdown, oxidation and corrosion, these devices are difficult to use in a complex environment [34]. Therefore, it is significant to develop tunable metasurfaces using all-dielectric structures. Based on the above factors, HOU *et al*. proposed a transmission LTC polarization converter by using a silicon metasurface. They deposited InSb film on the silica substrate and doped silicon as the structure material, which can control the polarization converter dynamically [35]. However, the fabrication of silicon pillars is complicated in the experiment, and the silicon is too fragile, which makes it difficult to storage in the experiment.

The structure of the microspheres presented in this paper is simpler in the fabrication process, and can be fabricated on a large scale, more economic, and easier to storage. Taking into account the above facts, it is significant for the development of terahertz science to realize the tunable terahertz polarization converter with simple structure, high bandwidth and large-scale fabrication by using all-dielectric metasurface.

In this work, a thermally tunable LTC polarization converter is proposed by using the active all-dielectric metasurface. The device includes zirconium oxide (ZrO_2) microsphere resonators, active strontium titanate (STO) cladding, and flexible polyimide substrate, enabling the large-scale fabrication [36]. This structure can dynamically convert the linearly polarized wave into right-hand circular polarization (RHCP) wave. At room temperature, numerical simulations indicate that the absolute value of axis ratio (AR) more than (≥) –3 dB and ellipticity less than (≤) –0.8 is realized in the frequency range of 0.247–0.278 THz (relative bandwidth is 12%). Obviously, the conversion frequency of the perfect RHCP wave has a blue-shift from 0.220 to 0.291 THz when the temperature changes from 200 to 380 K. Meanwhile, a great ellipticity modulation depth of 92% is observed at 0.220 THz, which demonstrates that the polarization state of output THz wave can be actively tuned. This platform with powerful THz functions proposed here will be widely used in tunable THz devices and has the great potential in 6G wireless communication.

2. Theoretical design and results in discussion

The diagram of the reported converter is illustrated in Fig. 1(a), which can realize the conversion from THz linear polarization wave to circular polarization state. As the unit

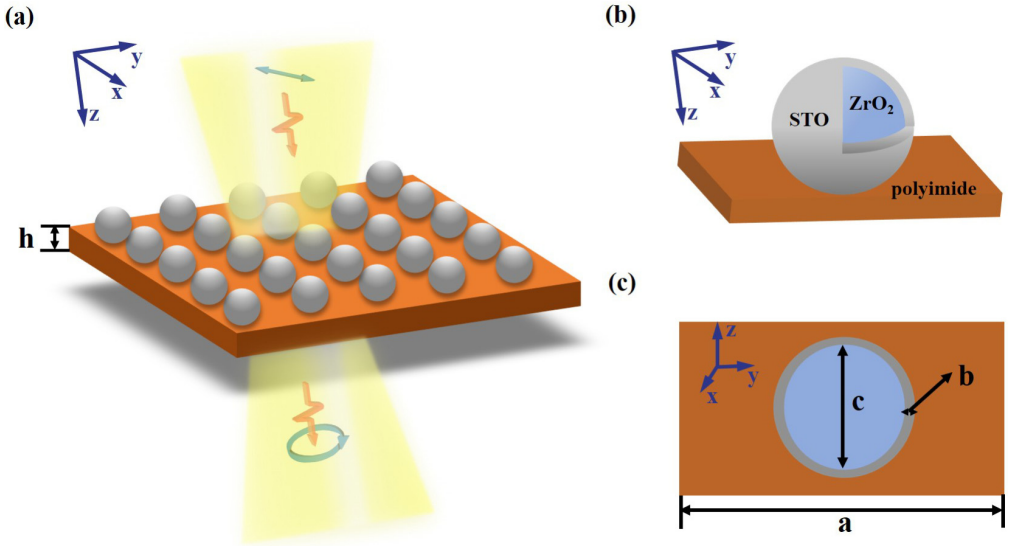

Fig. 1. (a) Illustration of the designed all-dielectric polarization conversion metasurface. (b) Graphical representation of structural elements. (c) Geometric parameters in the vertical view of structural unit cell.

cell indicated in Fig. 1(b), the converter is composed of ZrO_2 microsphere resonators, active STO cladding, and flexible polyimide substrate. Considering the stronger Mie -resonance in the high dielectric material, the ZrO_2 (ε = 40, loss tangent = 0.15) microsphere is selected as the resonator to control the electromagnetic characteristics of the THz wave [37]. To improve the flexibility of the converter, a 50 μm thick (h) polyimide (ε = 3.6, loss tangent = 0.01) is used as the substrate [36]. The active material STO (ε = 296, loss tangent = 0.015) is coated on the microsphere resonator to achieve the tunable ability of the polarization converter. The frequencies and the strength of the Mie resonance can be tuned effectively, and the change of the permittivity of the active material will cause the change of the permittivity of the whole structure, which will affect the Mie resonance accordingly [38]. Thus, the permittivity of STO changes with temperature, and the dynamic range of permittivity changes is higher, so the frequency range of its tuning is wider in the process of thermal tuning. Therefore, STO is chosen as the active material in this design. Furthermore, the proposed polarization converter parameters are selected through simulation optimization: a = 250 μm, b = 5 μm, c = 50 μm, as the vertical view of the converter is shown in Fig. 1(c).

We use CST Microwave Studio to simulate the performance of the polarization converter, and the unit cell boundary condition is used in the parameter setting. The transmission wave can be expressed as $E_t = E_{xt}\mathbf{e}_x + E_{yt}\mathbf{e}_y = t_{xx}\exp(j\varphi_{xx})E_{xi}\mathbf{e}_x + + t_{yy}\exp(j\varphi_{yy})E_{yi}\mathbf{e}_y$, where $t_{xx} = |E_{xt}/E_{xi}|$ and $t_{yy} = |E_{yt}/E_{yi}|$. In these equations, t_{xx}, t_{yy}, φ_{xx}, φ_{yy} represent the amplitude and phase of the x-to-x and y-to-y polarization conversion, respectively [39,40]. From the previous research, when $t_{xx} = t_{yy}$ and $\Delta\varphi = = \varphi_{yy} - \varphi_{xx} = 2n\pi \pm \pi/2$ (n is an integer) are achieved simultaneously, the perfect LTC polarization conversion function can be achieved, and "–" and "+" represent perfect RHCP wave and left-hand circular polarization (LHCP) wave [41]. Figures 2(a) and (b) describe the transmission amplitude and phase of x-to-x and y-to-y conversion, respectively. Furthermore, the difference between the orthogonal components is plotted in Fig. 2(c) to verify the correctness of the above equation. As the black and red curve is shown in Fig. 2(c), the amplitude of the orthogonal components is equal and the phase has the 270° difference at 0.265 THz. Combined with the theoretical analysis, we can speculate that the designed metasurface can indeed realize the LTC polarization conversion. In addition, the Stokes parameters are introduced by Eq. (1) and Eq. (2) to represent the ellipticity of the converter [42–44].

$$I = |t_{xx}|^2 + |t_{yy}|^2 \tag{1}$$

$$V = 2|t_{xx}||t_{yy}|\sin\Delta\varphi \tag{2}$$

The normalized ellipticity calculated by V/I is used to verify the performance of the converter. Here, V/I = +1 and V/I = –1 indicate the perfect LHCP and perfect RHCP wave. Based on the equation mentioned above, the ellipticity of the polarization converter is plotted in Fig. 2(d). It can be found that the ellipticity is close to –1 at 0.265 THz, which means the perfect transmission RHCP wave is realized. Meanwhile,

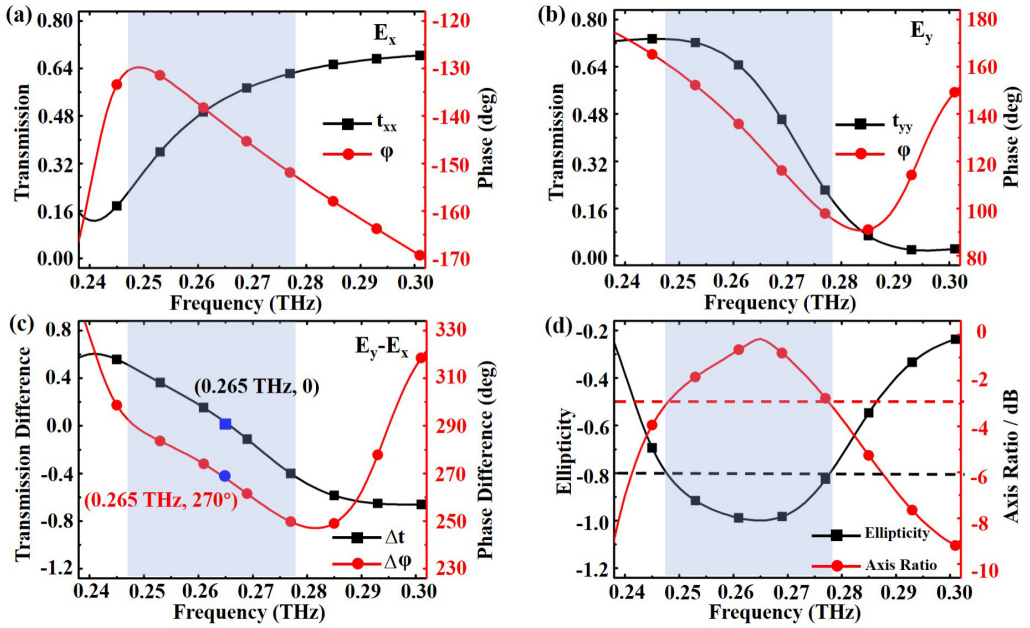

Fig. 2. Simulation results of the designed structure. (a) The *x*-polarized transmission THz wave magnitude and phase distribution. (b) The *y*-polarized transmission THz wave magnitude and phase. (c) The simulated amplitude and phase difference of *x*-polarized and *y*-polarized. (d) The ellipticity and axis ratio of the designed structure under the 45°-polarized incidence wave. (Incident angle: parallel to the *Z* axis, polarization angle: 45°, temperature: 300 K.)

we can find that from 0.247 to 0.278 THz (the blue region in Fig. 2(d)), the ellipticity is less than –0.8 with a bandwidth of 0.031 THz.

$$\beta = 0.5 \arcsin(V/I) \tag{3}$$

$$\mathrm{AR} = 10 \log(\tan\beta) \tag{4}$$

Except for ellipticity, the AR of the transmission can be obtained from Eqs. (3) and (4) [45]. The AR of the proposed polarization converter is more than –3 dB at the frequency of 0.247–0.278 THz with relative bandwidth of 12% (Fig. 2(d)). The calculated AR matches well with the ellipticity, *i.e.*, the structure performs excellent LTC polarization conversion within the frequency range covered by the blue shadow. Furthermore, the operating frequency indicates that the converter has broad application prospects in 6G wireless communication.

To give a detailed analysis of the electromagnetic response mechanism, the electric field distribution under 45° polarization incident wave is also studied. The simulated electric fields in different time phases are shown in Fig. 3. We can observe a strong electric field symmetrically distributed on the microspheres, and a very obvious magnetic resonance is observed inside the converter. The strong electric field resonance inside the microsphere leads to the realization of the polarization conversion function.

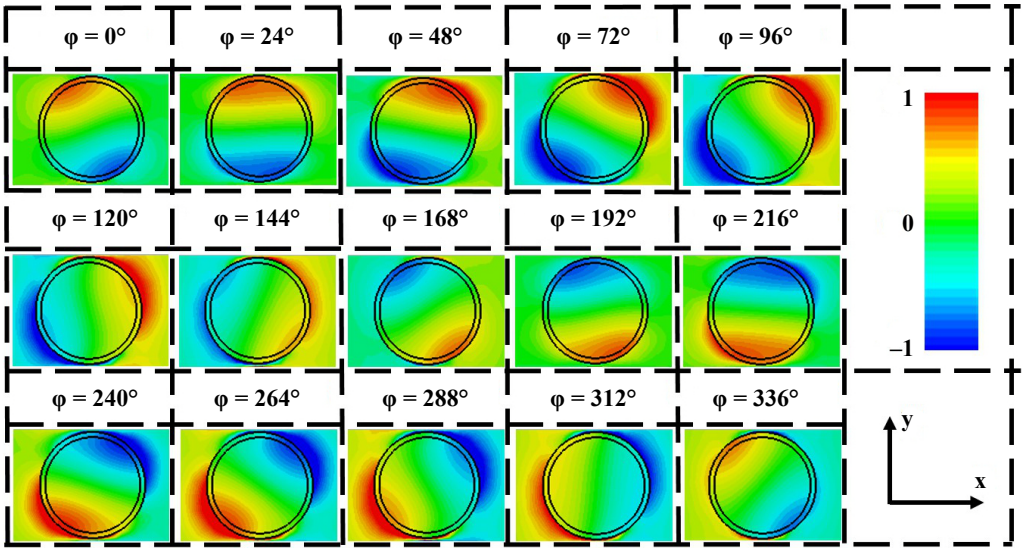

Fig. 3. The electric field distribution of the time phase varies from 0° to 336° under the excitation of the 45° polarized wave.

In addition, the spiral electric field distribution is obtained when the time phase is increased from 0° to 336°. Therefore, we can conclude that a perfect RHCP wave is achieved in our design. This result is consistent with the theoretical calculation and simulation results.

Next, the effects of the geometric parameters on the LTC polarization conversion performance are simulated. A slight blue shift of 0.005 THz is observed in Fig. 4(a) with the increase of the period. Meanwhile, the amplitude of ellipticity continues to approach –1 along with the blueshift of the resonance frequency. This phenomenon indicates that better conversion performance can be achieved by selecting the appropriate period. Besides, the relationship of the transmission ellipticity and microsphere radius is plotted in Fig. 4(b). A redshift of about 0.139 THz in the ellipticity dip is observed when the microsphere radius increases from 35 to 65 μm. Different from the trend that changes with the period, the amplitude of the ellipticity first continues to approach –1 (from 35 to 55 μm), and then begins to decrease (from 55 to 65 μm). This may result from the huge influence of radius on the anisotropy of the structure.

$$\gamma = \frac{1}{2}\left[\left|t_{xx}\right|^4 + \left|t_{yy}\right|^4\right] \tag{5}$$

Furthermore, the transmission efficiency of converters with different geometric parameters is also simulated and calculated according to Eq. (5). Figure 4(c) shows that the transmission efficiency is related to period. In Fig. 4(d) the dependence of the transmission efficiency on the radius is plotted. It can be seen that the transmission efficiency increases by 9% (from 24% to 33%) with the increases of the period (210–270 μm).

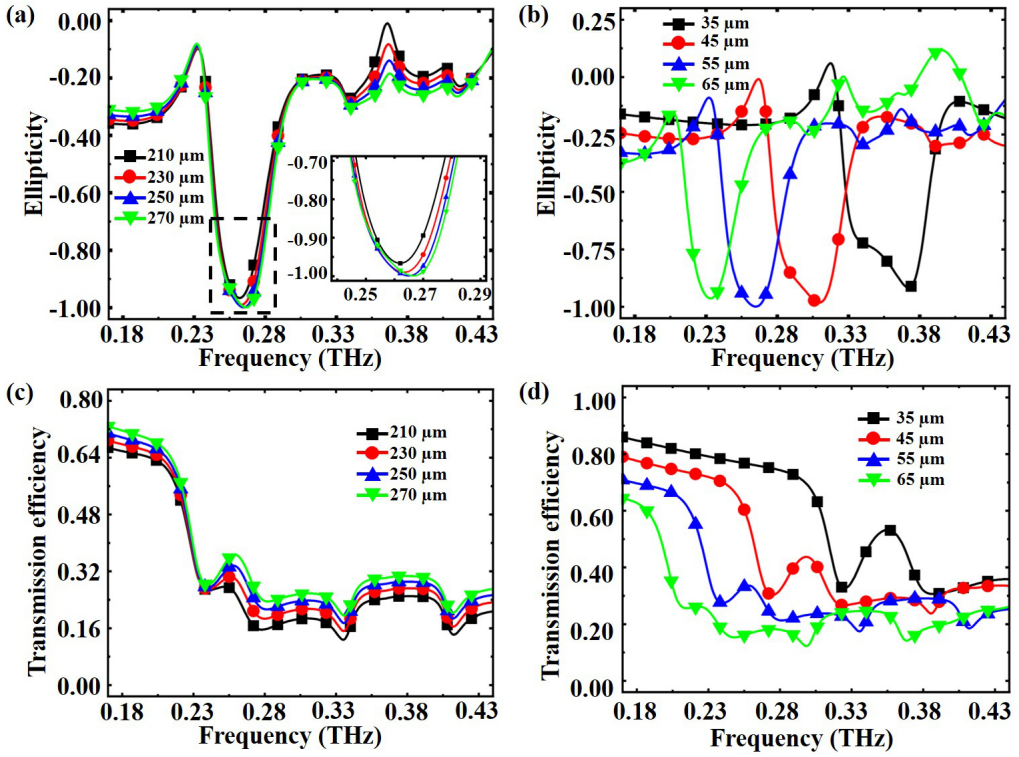

Fig. 4. The performance of the LTC converter is related to period and radius. (a) The relationship of the ellipticity and period. The inset shows the ellipticity from 0.24 to 0.29 THz. (b) The microsphere radius -dependent ellipticity. (c) The period-dependent transmission efficiency. (d) The microsphere radius-dependent transmission efficiency. (Incident angle: parallel to the *Z* axis, polarization angle: 45°, temperature: 300 K.)

Combined with the fact that the ellipticity continues to approach –1 as the increase of period, we can conclude that the larger period brings about better conversion performance. In contrast, the transmission efficiency of the polarization converter undergoes a gradual decrease from 40% to 23% when the radius varies from 25 to 65 μm. In this condition, considering the ellipticity and transmission efficiency comprehensively, there is an inflection point to improve the performance of the converter as the radius increases. It is stated above that both the period and the microsphere radius have a certain influence on the performance of LTC polarization conversion. Combining the influence of period and radius at the same time, the best geometric parameters are selected and taken in Fig. 1 as an example.

The dependence of the polarization performances on the incidence state of THz wave is also analysed. As shown in Fig. 5, the incident and polarization angles are also investigated. Figure 5(a) exhibits the profile of the ellipticity amplitude with the incident angle varying from 0° to 85° in a step of 5°. It can be seen that the amplitude of ellipticity is always less than –0.8 from 0.248 to 0.277 THz. It is apparent that the proposed

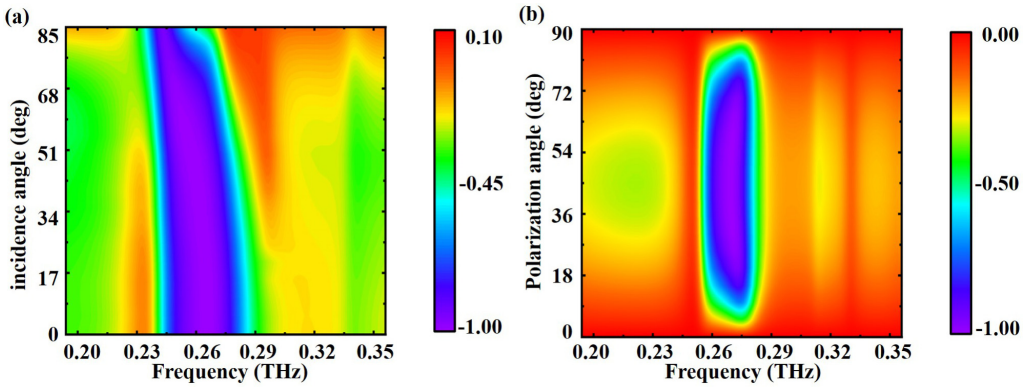

Fig. 5. (a) Simulated transmission ellipticity map under different incidence angle of THz wave. (b) Numerical simulated transmission ellipticity map under different polarization angle of THz wave.

converter is insensitive to the incident angle. Correspondingly, Fig. 5(b) shows the simulated amplitude of ellipticity dependence on the polarization angle, with the polarization angle changing from 0° to 90° in a step of 5°. The results obtained from this graph show that the amplitude of the ellipticity is divided by the polarization angle of 45°. The reason of this phenomenon is that the electric field components of x and y directions are exactly equal under the 45° polarized waves. Then along with the angle increases or decreases, the symmetry of the structure leads to the symmetry of the spectrum. Furthermore, when the polarization angle increases from 10° to 80°, the amplitude of ellipticity is always less than –0.8 at 0.029 THz (from 0.248 to 0.277 THz). The insensitivity of the converter to the incident and polarization angle brings greater freedom for structural application.

After investigating the geometrical parameters of the converter and the angle of the THz wave, the tunability of the converter is researched to expand its applications. As we all know, as the active ferroelectric material, the permittivity of the STO can be calculated with the Drude model [46–48]:

$$\varepsilon_\omega = \varepsilon_\infty + f/(\omega_0^2 - \omega^2 - i\omega\gamma) \tag{6}$$

Here, $\varepsilon_\infty \approx 9.6$ is high-frequency bulk permittivity, $f = 2.3 \times 10^6$ cm^2 is the oscillator strength, and ω is the working angular frequency in the THz band. Besides these parameters, the soft mode frequency ω_0 and damping parameter γ can be expressed as:

$$\omega_0(T)[\mathrm{cm}^{-1}] = \sqrt{31.2(T - 42.5)} \tag{7}$$

$$\gamma(T)[\mathrm{cm}^{-1}] = -3.3 + 0.094\,T \tag{8}$$

Through the temperature-dependent parameters ω_0 and γ in Eq. (7) and Eq. (8), we can speculate the permittivity of STO under different temperatures and study its influence on the converter. The real part of the permittivity at different temperatures is

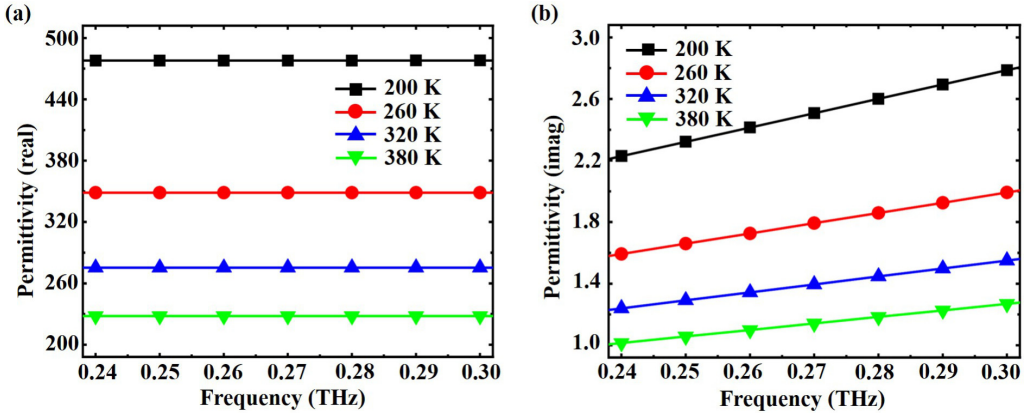

Fig. 6. The permittivity of strontium titanate is calculated by the Drude model. (a) The real part of the strontium titanate permittivity. (b) The imaginary part of the strontium titanate permittivity.

shown by various graphical curves in Fig. 6(a). It can be seen that when the temperature decreases from 380 to 200 K, the real part of permittivity increases from 228 to 479. Meanwhile, the decrease of the imaginary part of the permittivity observed in Fig. 6(b) indicates the relationship between loss and temperature. These results show the potential application of STO materials in the active THz devices. The change of the STO permittivity will influence the dielectric properties of the resonator. That is why the STO is selected to be coated on the microspheres to realize the tunable THz LTC polarization converter.

In order to verify the above speculation, the variation of ellipticity with the increase of temperature is simulated. The simulated amplitude of the ellipticity with temperature to achieve a frequency regulation of 0.220 to 0.291 THz is plotted in Fig. 7(a). A frequency blueshift of about 0.071 THz (0.220–0.291 THz) is observed with the temper-

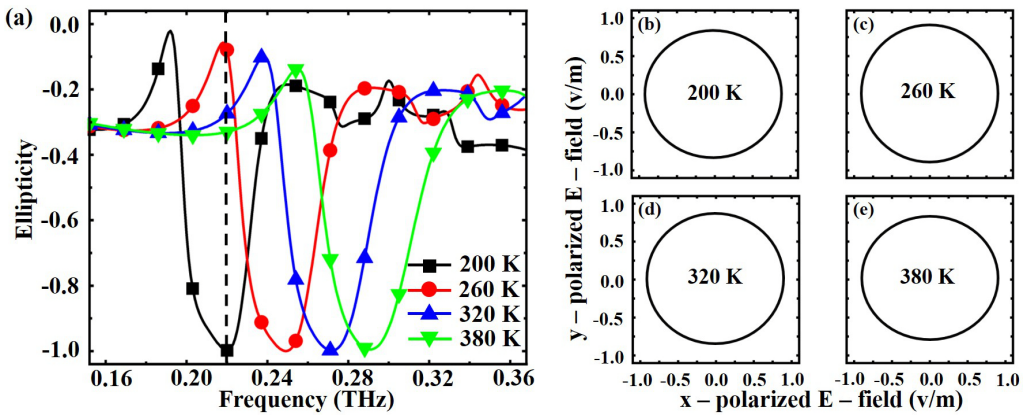

Fig. 7. (a) The amplitude of the ellipticity with the increase of temperature. (b)–(e) The electric field trajectory diagram for ellipticity at different temperatures.

ature rising from 200 to 380 K. The corresponding electric field trajectory diagram is plotted in Fig. 7(b), the ideal circles demonstrate the perfect polarization conversion performance in the tunable process. In addition, the sensitivity $((f_{max} - f_{min})/(T_{max} - T_{min}))$ of the proposed tunable converter is about 39 GHz/100 K. Meanwhile, the modulation depth of the ellipticity amplitude can achieve 92% (from 7.97% to 99.78%) at 0.220 THz. It is obvious that the polarization state of the output electromagnetic wave can also be controlled. This finding means that the proposed converter cannot be limited in the application of circular polarization, which effectively increases its scope of application. For the better performance of the tunable polarization converter, we believe it has more potential in beam control, wireless communications, and other functional devices.

3. Conclusions

In conclusion, a thermally tunable LTC polarization converter is proposed based on the STO all-dielectric metasurface at THz frequency. Because the proposed design has thermal stimulation tuning characteristics, a tunable operating band can be obtained. At room temperature, the proposed LTC polarization converter has an ellipticity amplitude of –1 at 0.265 THz, which indicates that a perfect RHCP wave is achieved. In addition, the amplitude of the ellipticity is less than –0.8 and the AR is greater than –3 dB, when the frequency is between 0.247 and 0.278 THz (relative bandwidth is 12%). More importantly, with a temperature rise of 180 K (from 200 to 380 K), the LTC polarization converter can tune the conversion frequency of the RHCP wave from 0.220 to 0.291 THz. And an ellipticity modulation depth of 92% is observed at 0.220 THz. The LTC converter is one of the most basic functions of optical components, which plays a significant role in the development of wireless communication.

Acknowledgements

This work was supported by National Key R&D Program of China (2019YFB2203104, 2020YFB2205801); National Natural Science Foundation of China (NSFC) (61805231, 11974058); Beijing Nova Program (Z201100006820125) from Beijing Municipal Science and Technology Commission; Beijing Natural Science Foundation (Z210004); and State Key Laboratory of Information Photonics and Optical Communications (IPOC2021ZT01), BUPT, China.

References

[1] JEPSEN P.U., COOKE D.G., KOCH M., *Terahertz spectroscopy and imaging–Modern techniques and applications*, Laser & Photonics Reviews **5**(1), 2011, pp. 124–166, DOI: 10.1002/lpor.201000011.

[2] KATLETZ S., PFLEGER M., PÜHRINGER H., MIKULICS M., VIEWEG N., PETERS O., SCHERGER B., SCHELLER M., KOCH M., WIESAUER K., *Polarization sensitive terahertz imaging: detection of birefringence and optical axis*, Optics Express **20**(21), 2012, pp. 23025–23035, DOI: 10.1364/OE.20.023025.

[3] TONOUCHI M., *Cutting-edge terahertz technology*, Nature Photonics **1**(2), 2007, pp. 97–105, DOI: 10.1038/nphoton.2007.3.

[4] SONG Z., GAO Z., ZHANG Y., ZHANG B., *Terahertz transparency of optically opaque metallic films*, Europhysics Letters **106**(2), 2014, article no. 27005, DOI: 10.1209/0295-5075/106/27005.

[5] Fahad A. K., Ruan C., Chen K., *Dual-wide-band dual polarization terahertz linear to circular polarization converters based on bi-layered transmissive metasurfaces*, Electronics **8**(8), 2019, article no. 869, DOI: 10.3390/electronics8080869.
[6] Fellers R.S., Leforestier C., Braly L.B., Brown M.G., Saykally R.J., *Spectroscopic determination of the water pair potential*, Science **284**(5416), 1999, pp. 945–948, DOI: 10.1126/science.284.5416.945.
[7] Ho L., Pepper M., Taday P., *Signatures and fingerprints*, Nature Photonics **2**(9), 2008, pp. 541–543, DOI: 10.1038/nphoton.2008.174.
[8] Jansen C., Wietzke S., Peters O., Scheller M., Vieweg N., Salhi M., Krumbholz N., Jordens C., Hochrein T., Koch M., *Terahertz imaging: applications and perspectives*, Applied Optics **49**(19), 2010, pp. E48–E57, DOI: 10.1364/AO.49.000E48.
[9] Woodward R.M., Wallace V.P., Pye R.J., Cole B.E., Arnone D.D., Linfield E.H., Pepper M., *Terahertz pulse imaging of* ex vivo *basal cell carcinoma*, Journal of Investigative Dermatology **120**(1), 2003, pp. 72–78, DOI: 10.1046/j.1523-1747.2003.12013.x.
[10] Nagatsuma T., Horiguchi S., Minamikata Y., Yoshimizu Y., Hisatake S., Kuwano S., Yoshimoto N., Terada J., Takahashi H., *Terahertz wireless communications based on photonics technologies*, Optics Express **21**(20), 2013, pp. 23736–23747, DOI: 10.1364/OE.21.023736.
[11] Koenig S., Lopez-Diaz D., Antes J., Boes F., Henneberger R., Leuther A., Tessmann A., Schmogrow R., Hillerkuss D., Palmer R., Zwick T., Koos C., Freude W., Ambacher O., Leuthold J., Kallfass I., *Wireless sub-THz communication system with high data rate*, Nature Photonics **7**(12), 2013, pp. 977–981, DOI: 10.1038/nphoton.2013.275.
[12] Qiu F., Tan Z., Fu Z., Wan W., Li M., Wang C., Cao J., *Reflective scanning imaging based on a fast terahertz photodetector*, Optics Communications **427**, 2018, pp. 170–174, DOI: 10.1016/j.optcom.2018.06.030.
[13] Li J., *A novel terahertz wave reflective polarizer for THz communication*, Optics Communications **284**(4), 2011, pp. 957–960, DOI: 10.1016/j.optcom.2010.10.020.
[14] Liu M., Tian Z., Zhang X., Gu J., Ouyang C., Han J., Zhang W., *Tailoring the plasmon-induced transparency resonances in terahertz metamaterials*, Optics Express **25**(17), 2017, pp. 19844–19855, DOI: 10.1364/OE.25.019844.
[15] Zhao R., Zhang L., Zhou J., Koschny Th., Soukoulis C.M., *Conjugated gammadion chiral metamaterial with uniaxial optical activity and negative refractive index*, Physical Review B **83**(3), 2011, article no. 035105, DOI: 10.1103/PhysRevB.83.035105.
[16] Chang C., Chen H., *Broadband terahertz linear-to-circular polarization conversion*, [In] *2018 43rd International Conference on Infrared, Millimeter, and Terahertz Waves* (*IRMMW-THz*), IEEE, 2018, pp. 1–3, DOI: 10.1109/IRMMW-THz.2018.8510418.
[17] Xia R., Jing X., Zhu H., Wang W., Tian Y., Hong Z., *Broadband linear polarization conversion based on the coupling of bilayer metamaterials in the terahertz region*, Optics Communications **383**, 2017, pp. 310–315, DOI: 10.1016/j.optcom.2016.08.060.
[18] Lee W.S.L., Nirantar S., Headland D., Bhaskaran M., Sriram S., Fumeaux C., Withayachumnankul W., *Broadband terahertz circular-polarization beam splitter*, Advanced Optical Materials **6**(3), 2018, article no. 1700852, DOI: 10.1002/adom.201700852.
[19] Masson J.-B, Gallot G., *Terahertz achromatic quarter-wave plate*, Optics Letters **31**(2), 2006, pp. 265–267, DOI: 10.1364/OL.31.000265.
[20] You X., Fumeaux C., Withayachumnankul W., *Broadband terahertz quarter-wave plate design*, [In] *2019 44th International Conference on Infrared, Millimeter, and Terahertz Waves* (*IRMMW-THz*), IEEE, 2019, pp. 1–2, DOI: 10.1109/IRMMW-THz.2019.8874192.
[21] Minovich A.E., Miroshnichenko A.E., Bykov A.Y., Murzina T.V., Neshev D.N., Kivshar Y.S., *Functional and nonlinear optical metasurfaces*, Laser & Photonics Reviews **9**(2), 2015, pp. 195–213, DOI: 10.1002/lpor.201400402.
[22] Martini E., Mencagli M., Maci S., *Metasurface transformation for surface wave control*, Philosophical Transactions of the Royal Society A: Mathematical, Physical and Engineering Sciences **373**(2049), 2015, article no. 20140355, DOI: 10.1098/rsta.2014.0355.

[23] ZHANG Y., LI T., CHEN Q., ZHANG H., O'HARA J.F., ABELE E., TAYLOR A.J., CHEN H.T., AZAD A.K., *Independently tunable dual-band perfect absorber based on graphene at mid-infrared frequencies*, Scientific Reports **5**(1), 2015, article no. 18463, DOI: 10.1038/srep18463.

[24] WANG J., GAO C.N., JIANG Y.N., AKWURUOHA C.N., *Ultra-broadband and polarization-independent planar absorber based on multilayered graphene*, Chinese Physics B **26**(11), 2017, article no. 114102, DOI: 10.1088/1674-1056/26/11/114102.

[25] WANG J., JIANG Y., *Infrared absorber based on sandwiched two-dimensional black phosphorus metamaterials*, Optics Express **25**(5), 2017, pp. 5206–5216, DOI: 10.1364/OE.25.005206.

[26] WANG J., JIANG Y., HU Z., *Dual-band and polarization-independent infrared absorber based on two-dimensional black phosphorus metamaterials*, Optics Express **25**(18), 2017, pp. 22149–22157, DOI: 10.1364/OE.25.022149.

[27] GRADY N.K., HEYES J.E., CHOWDHURY D.R., ZENG Y., REITEN M.T., AZAD A.K., TAYLOR A.J., DALVIT D.A.R., CHEN H.T., *Terahertz metamaterials for linear polarization conversion and anomalous refraction*, Science **340**(6138), 2013, pp. 1304–1307, DOI: 10.1126/science.1235399.

[28] CHIANG Y., YEN T., *A composite-metamaterial-based terahertz-wave polarization rotator with an ultrathin thickness, an excellent conversion ratio, and enhanced transmission*, Applied Physics Letters **102**(1), 2013, article no. 011129, DOI: 10.1063/1.4774300.

[29] ZHU L., DONG L., GUO J., MENG F.Y., HE X.J., ZHAO C.H., WU Q., *Polarization conversion based on Mie-type electromagnetically induced transparency (EIT) effect in all-dielectric metasurface*, Plasmonics **13**(6), 2018, pp. 1971–1976, DOI: 10.1007/s11468-018-0712-8.

[30] ZHU J., LI S., DENG L., ZHANG C., YANG Y., ZHU H., *Broadband tunable terahertz polarization converter based on a sinusoidally-slotted graphene metamaterial*, Optical Materials Express **8**(5), 2018, pp. 1164–1173, DOI: 10.1364/OME.8.001164.

[31] XIAO Z., ZOU H., ZHENG X., LING X., WANG L., *A tunable reflective polarization converter based on hybrid metamaterial*, Optical and Quantum Electronics **49**(12), 2017, article no. 401, DOI: 10.1007/s11082-017-1235-9.

[32] ZHAO X., SCHALCH J., ZHANG J., SEREN H.R., DUAN G., AVERITT R.D., ZHANG X., *Electromechanically tunable metasurface transmission waveplate at terahertz frequencies*, Optica **5**(3), 2018, pp. 303–310, DOI: 10.1364/OPTICA.5.000303.

[33] VASIĆ B., ZOGRAFOPOULOS D.C., ISIĆ G., BECCHERELLI R., GAJIĆ R., *Electrically tunable terahertz polarization converter based on overcoupled metal-isolator-metal metamaterials infiltrated with liquid crystals*, Nanotechnology **28**(12), 2017, article no. 124002, DOI: 10.1088/1361-6528/aa5bbd.

[34] YANG X., ZHANG D., WU S., YIN Y., LI L., CAO K., HUANG K., *Reconfigurable all-dielectric metasurface based on tunable chemical systems in aqueous solution*, Scientific Reports **7**(1), 2017, article no. 3190, DOI: 10.1038/s41598-017-03439-9.

[35] HOU Y., ZHANG C., WANG C., *High-efficiency and tunable terahertz linear-to-circular polarization converters based on all-dielectric metasurfaces*, IEEE Access **8**, 2020, pp. 140303–140309, DOI: 10.1109/ACCESS.2020.3007838.

[36] YANG D., ZHANG C., JU X., JI Y., LAN C., *Multi-resonance and ultra-wideband terahertz metasurface absorber based on micro-template-assisted self-assembly method*, Optics Express **28**(2), 2020, pp. 2547–2556, DOI: 10.1364/OE.381927.

[37] BI K., YANG D., CHEN J., WANG Q., WU H., LAN C., YANG Y., *Experimental demonstration of ultra-large-scale terahertz all-dielectric metamaterials*, Photonics Research **7**(4), 2019, pp. 457–463, DOI: 10.1364/PRJ.7.000457.

[38] LAN C., MA H., WANG M., GAO Z., LIU K., BI K., ZHOU J., XIN X., *Highly efficient active all-dielectric metasurfaces based on hybrid structures integrated with phase-change materials: from terahertz to optical ranges*, ACS Applied Materials and Interfaces **11**(15), 2019, pp. 14229–14238, DOI: 10.1021/acsami.8b22466.

[39] ZHANG L., ZHOU P., LU H., ZHANG L., XIE J., DENG L., *Realization of broadband reflective polarization converter using asymmetric cross-shaped resonator*, Optical Materials Express **6**(4), 2016, pp. 1393–1404, DOI: 10.1364/OME.6.001393.

[40] Jiang Y., Wang L., Wang J., Akwuruoha C.N., Cao W., *Ultra-wideband high-efficiency reflective linear-to-circular polarization converter based on metasurface at terahertz frequencies*, Optics Express **25**(22), 2017, pp. 27616–27623, DOI: 10.1364/OE.25.027616.
[41] Zahn M., *Electromagnetic Field Theory: A Problem Solving Approach*, Krieger, 2003.
[42] Li Y., Zhang J., Qu S., Wang J., Zheng L., Pang Y., Xu Z., Zhang A., *Achieving wide-band linear -to-circular polarization conversion using ultra-thin bi-layered metasurfaces*, Applied Physics **117**(4), 2015, article no. 044501, DOI: 10.1063/1.4906220.
[43] Gao X., Yu X.-Y., Cao W.-P., Jiang Y.-N., Yu X.-H., *Ultra-wideband circular-polarization converter with micro-split Jerusalem-cross metasurfaces*, Chinese Physics B **25**(12), 2016, article no. 128102, DOI: 10.1088/1674-1056/25/12/128102.
[44] Cong L., Cao W., Zhang X., Tian Z., Gu J., Singh R., Han J., Zhang W., *A perfect metamaterial polarization rotator*, Applied Physics Letters **103**(17), 2013, article 171107, DOI: 10.1063/1.4826536.
[45] Zhang H., Zeng L., Liu G., Huang T., *Tunable linear-to-circular polarization converter using the graphene transmissive metasurface*, IEEE Access **7**, 2019, pp. 158634–158642, DOI: 10.1109/ACCESS.2019.2950847.
[46] Huang X., He W., Yang F., Ran J., Yang Q., Xie S., *Thermally tunable metamaterial absorber based on strontium titanate in the terahertz regime*, Optical Materials Express **9**(3), 2019, pp. 1377–1385, DOI: 10.1364/OME.9.001377.
[47] Li W., Cheng Y., *Dual-band tunable terahertz perfect metamaterial absorber based on strontium titanate* (*STO*) *resonator structure*, Optics Communications **462**, 2020, article no. 125265, DOI: 10.1016/j.optcom.2020.125265.
[48] Zhan Y., Li B., Lan C., Bi K., Qu Z., *Tunable silicon-based all-dielectric metamaterials with strontium titanate thin film in terahertz range*, Optics Express **25**(18), 2017, pp. 22158–22163, DOI: 10.1364/OE.25.022158.

Received November 24, 2021
in revised form February 17, 2022